Lasers in Manufacturing Conference 2015

Adjustment of surface energy on steel surfaces due to CLP generation by picosecond laser processing

Tom Häfner[a,b]*, Johannes Heberle[a,b], Daniel Holder[a], Michael Schmidt[a,b]

[a]*Friedrich-Alexander-University Erlangen-Nürnberg (FAU), Institute of Photonic Technologies, Konrad-Zuse-Straße 3-5, 91052 Erlangen, Germany*

[b]*Erlangen Graduate School in Advanced Optical Technologies (SAOT), Friedrich-Alexander-University Erlangen-Nürnberg (FAU), Germany*

Abstract

With regard to mechanical and chemical resistivity metal surfaces can benefit from hydrophobic behavior. Against this background, results of laser-induced generation of hydrophobic surfaces on three different steel alloys without any additional coating are presented. Therefore, a dual-scale structure - consisting of micro cones and nano-ripples and droplets - is generated by picosecond laser structuring in ambient air.

Firstly, the dependencies of the formation of these micro cones, called cone-like protrusions (CLP), on different parameters of the laser ablation process - the peak fluence, the spot diameter, the effective pulse number per unit area and the material - are investigated. Secondly, the hydrophobicity and surface energy of the resulting surface topography of the irradiated substrate are evaluated by means of contact angle measurements. For that purpose identical topographies are generated on stainless steel, hot- and cold-working steel. The time-dependency of the contact angle is investigated depending on the material and the morphology.

For CLP formation a high number of scans is preferred to provide a high effective pulse number per unit area, which is advantageous for homogeneous generation of larger micro cones. By measuring the contact angle a change from an initially hydrophilic to a hydrophobic behavior of the surfaces can be observed due to a change of surface chemistry over time. Thus, contact angles higher than 90° can be measured on laser treated surfaces of different steel alloys.

Keywords: Micro processing; ablation; surface functionalization; steel alloy

*Corresponding author. Tel.: +49-9131-85-23244; fax: +49-9131-85-23234.
E-mail address: tom.haefner@fau.de.

1. Introduction

Friction and wear mechanisms are significantly influenced by morphological and chemical properties of the contacting surfaces within tribological systems. The surface energy - influenced by the chemical properties - can affect adhesive friction and wear [1]. Thus, friction can be changed due to an adjustment of the surface energy. A lower surface energy contributes the prevention of adhesions and by this the generation of wear particles or other material residues which can cause abrasive wear of tool surfaces [2]. Furthermore, hydrophobic surfaces can benefit from anti-corrosive behavior [3].

1.1. Hydrophobic surfaces on metals

The hydrophobicity of a surface is influenced by the combination of its chemical and morphological characteristics [4]. The surface morphology influences the wettability either in hydrophilic or in hydrophobic state. Wettability and in particular hydrophobicity is usually assessed by the contact angle of a droplet of distilled water. Depending on the wettability two models exist to describe wetting of rough or chemically inhomogeneous surfaces. The *Wenzel* model describes the wetting of a droplet on a rough surface with a homogeneous solid-liquid interface respectively without an air interlayer [5]. According to the *Wenzel* model the contact angle either increases in the hydrophobic state or decreases in the hydrophilic state due to an increasing roughness. However, this model would imply complete drying of the surface due to an extremely high roughness, which cannot be observed in reality [6]. *Cassie-Baxter* extended this model to describe the wetting, which is characterized by a composite interface including a liquid-air- and solid-air-interface [7]. Thus, the *Cassie-Baxter* model describes the wetting of a rough surface with air-pockets (*Cassie* state).

The generation of hydrophobic or super-hydrophobic surfaces usually aims on the realization of surface topographies ensuring the *Cassie* state. For this reason, a micro- and nano-scaled morphology including a pillar-like topography with micro cones and nanostructures has to be achieved to provide air pockets below the droplet. To achieve contact angles $\theta > 150°$ (super-hydrophobicity) for the droplet radius $R = 1$ mm the dimensions of these cones can be calculated to: height $H = 30$ µm, width $B = 15$ µm and periodicity respectively mean distance $P = 145$ µm [8]. There are different single or combined approaches to realize dual-scale morphologies such as and sandblasting [4], electroless plating [9], lithography and wet etching [10].

1.2. Laser-based generation of hydrophobic surfaces

The research on laser-based generation of hydrophobic surfaces on metals is a subject of wide scientific interest [11]. These investigations follow different approaches regarding structure generation on different materials. In many studies, laser-processing is followed by a coating step, e.g. to silanise the surface, for the reduction of the surface energy of metals [12]. In the following, this possibility is not considered because the exclusive laser-based surface treatment allows the reduction of a process step and is of particular interest for large-scale tools such as rolls. Laser systems with pulse durations ranging from nanoseconds to femtoseconds are applied for single step laser-processing. Nanosecond-based texturing is mainly based on the sequential direct texturing to generate a periodic lattice-like topography aiming on the realization of the *Cassie* state [13]. In contrast, femtosecond-based texturing enables the processing with a higher productivity due to the generation of self-organized microstructures - called cone-like protrusions (CLP) [14]. Laser-texturing with pulse duration in the pico- or femtosecond range is characterized by a small heat-affected zone, which is advantageous regarding remaining constant surrounding material properties [15]. In both cases, hydrophobicity arises only with a certain time of delay after laser processing. This delay is necessary due to the deposition of carbon on the laser-processed surface, which causes the reduction of the surface energy [14].

The generation of CLP by picosecond laser processing to produce hydrophobic or super-hydrophobic surfaces is not investigated, yet. Due to the higher amount of arising melt compared to femtosecond ablation, CLP should be more efficiently induced. For this reason, the generation of higher CLP respectively higher surface roughness should be enabled. Thus, higher contact angles according to the *Cassie* state should be achievable. In the following chapters the influence of picosecond laser-textured surface morphology on the contact angle and the surface energy is investigated. The objective is the efficient generation of hydrophobic surfaces respectively low surface energies on selected steel alloys.

2. Methodology

2.1. Material properties

The wettability on laser-textured surfaces of three different steel alloys is investigated. The stainless steel 1.4301 is applied to investigate parameter dependencies of CLP formation and correlations between the surface morphology and the static contact angle θ. The hot-working steel 1.7229 and the cold-working steel 1.2379 are used to investigate the influence of the chemical composition of the steel alloy on the wettability. The chemical compositions and the thermal conductivities at room temperature of these steels are summarized in Tab. 1. Prior to laser processing all samples are manually ground to achieve a common roughness value $Sa = 0.04 \pm 0.01$ µm. After grinding, all samples are ultrasonically cleaned for 3 min in isopropanol to remove grinding residues.

Table 1. Chemical composition and thermo-physical properties of the investigated steel alloys [16,17,18]

Elemental composition in weight-%									Thermal conductivity k in W/(m*K) (at 20 °C)
Steel alloy	Fe	C	Si	Cr	Ni	Mn	Mo	V	
1.4301	69.00	≤ 0.07	≤ 1.00	17.50 - 19.50	8.00 - 15.00	≤ 2.00	-	-	15.0
1.7229	96.70	0.06	0.35	1.00	< 0.60	0.70	0.20	-	45.2
1.2379	84.75	1.55	-	12.00	-	-	0.80	0.90	16.7

2.2. Experimental setup for laser machining

The picosecond laser system Fuego (Time-Bandwidth Products) is applied for laser texturing. The emitted linear polarized laser light has a wavelength $\lambda = 1064$ nm. Enabling maximum heat accumulation without shielding effects due to plasma or particle plumes a pulse frequency $f_P = 200$ kHz is used [19]. The galvanometer scanner hurryScan 14 II (Scanlab AG) deflects the laser beam on the sample surface which is positioned at the beam waist w_0. The beam is focused by an F-theta lens with the focal length f = 160 mm. The size of the beam waist is varied by changing the beam diameter at the scanner aperture due to variable beam expanding.

2.3. Methods of surface characterization

After laser machining the textured surfaces are topographically characterized by means of measurements with a confocal laser scanning microscope (LSM) LEXT (Olympus). The surface roughness parameters are optically measured according to ISO 25178 with the LSM [20]. The scanning electron microscope (SEM) Merlin Gemini II (Zeiss) and its EDX tool are used to investigate the nanostructure and the chemical

composition of the untreated and textured surfaces. The surface wettability is assessed by measurements of the static contact angle θ with a self-built contact angle measurement device according to DIN 55660-2 [21]. For this purpose, a droplet of distilled water with V = 6 µl is applied on the sample surfaces. The surface energy is determined according to the method of Owens-Wendt-Ray-Kaelble (OWRK) [21]. The testing liquids are distilled water, ethylene glycol and glycerine. All textured and wet surfaces are quadratic with a side length of at least 7 mm. All samples are stored in a process chamber flooded by carbon dioxide at normal pressure.

3. Results and discussion

The results address the efficient generation of homogeneous cone-like protrusions (CLP) with the requirement of maximum height and width. Based on this, the influences of the laser-induced surface morphology and the chemical composition on the wetting behavior are discussed.

3.1. Influences on generation of ripples and CLP on stainless steel

For the generation of areal homogenous CLP of sufficient height according to the *Cassie-Baxter* model the necessary processing parameters are determined. The effective pulse number per unit area N_{eff} is derived out of results from *Liu et al.* [22]. They observed the maximum height of the CLP in the center of laser spot during ablation of craters with a pulse number of $N \approx 600$ in processing with a 10 ps laser. Based on *Tanvir Ahmmed et al.*, the effective pulse number per unit area N_{eff} for 2D scanning of the samples is calculated by eq. (1) [23]:

$$N_{eff} = S \times N_{eff,x} \times N_{eff,y} = S \times \frac{2 \times w_0}{\frac{v_S}{f_P}} \times \frac{2 \times w_0}{p_y} = S \times \frac{4 \times w_0 \times f_P}{v_S \times p_y} \qquad (1)$$

In this equation the following parameters are involved: number of scans S, beam waist radius w_0, pulse frequency f_P, scanning velocity v_S and the distance of the scanning lines p_y. According to the pulse number of $N \approx 600$ from *Liu et al.* the scanning velocity and the line distance are adjusted under the constraints of $w_0 = 16$ µm and $f_P = 200$ kHz. For the chosen line distance $p_y = 7.5$ µm - this distance ensures an even, non-wavy textured surface - the scanning velocity is set to $v_S = 45$ mm/s for S = 1 to find the regime of the peak fluence, which is relevant for homogeneous CLP generation. The peak fluence variation shows the expected result of surface texturing, which is characterized by different nano- and micro-scaled structures (Fig. 1). At comparatively low peak fluences $F_0 < 1.0$ J/cm² the textured area is homogeneously covered by ripples (laser-induced periodic surfaces structures, LIPSS) with a period of approximately 700 nm (Fig. 1a). Above a certain peak fluence cone-like protrusions (CLP or micro cones) locally start to form due to the residual and accumulated heat reaching the temperature threshold for self-organized cone formation (Fig. 1b) [24]. These micro cones are increasing in height, width and mean distance by increasing peak fluence, which coincidences with [22]. The nearly linear rising height can be explained by an increasing amount of melt due to the phase explosion, which is the dominating ablation mechanism in the strong phase ablation regime. The threshold of this regime for 1.4301 is experimentally determined to $F_0 = 2.6 \pm 0.3$ J/cm². The growth of the micro cones can be observed by the trend of selected surface roughness parameters, too (Fig. 2). The increase of the maximum surface height Sz and the reduced peak height Spk signalize growing micro cones. Furthermore, these parameters indicate the homogeneous distribution of the formed micro cones as both values start to

stagnate for $F_0 \geq 3.0$ J/cm². Together with the roughness parameter of the peak material portion Smr,1 (according to ISO 25178 [20]), which significantly drops at this peak fluence, they indicate the formation of homogeneous micro cones. In the case of homogeneous micro cones Smr,1 is about 15 %.

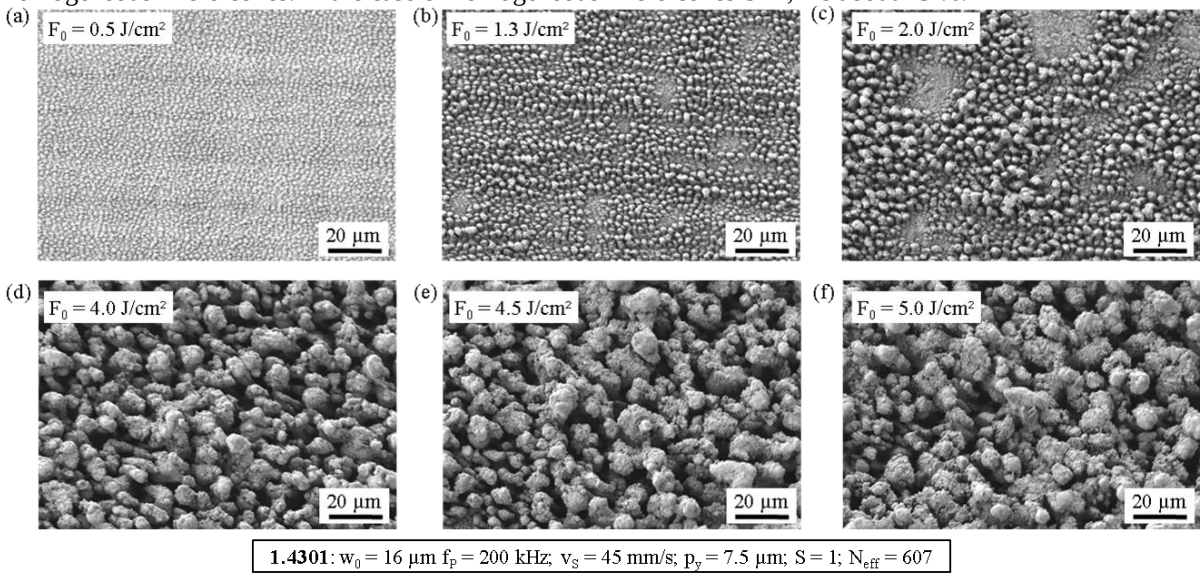

Fig. 1. Exemplary topographies of textured samples to estimate the distribution of generated nano- and micro-scale structures at different peak fluences

For peak fluences above 4.5 J/cm² the measured cone height H as well as the reduced peak height Spk show, that the cones are not rising further. At this fluence the maximum homogeneous distribution is reached (Fig. 1e). Higher fluences only lead to broader cones as it is observed in fs laser texturing, also [11].

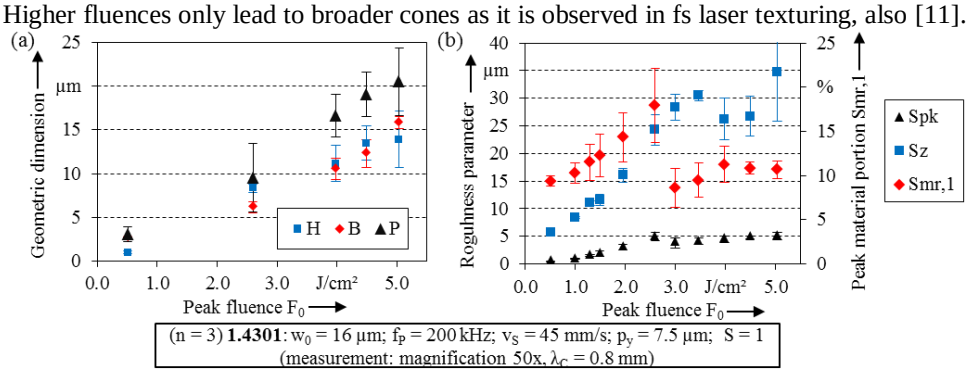

Fig. 2 (a) Height H, width B and mean distance P of the micro cones and (b) corresponding roughness parameters of the textured surfaces

The geometric dimensions H, B, P only cover the size of single micro cones and not their areal distribution. Therefore, in the further investigations on the optimization of the micro cone geometry evaluation is done by the surface roughness parameters.

Because the micro cones generated at $F_0 = 4.5$ J/cm² show a maximum homogeneous distribution and nearly maximum height, this peak fluence is applied in further investigations to increase the cones' height, width and mean distance to achieve a state similar to the *Cassie-Baxter* model. For this purpose, the effect on

scanning velocity and number of scans, acccordingly the effective pulse number per unit area is investigated. As the maximum scanning velocity for homogeneous formation of micro cones on 1.4301 is experimentally determined to v_S = 650 mm/s, this velocity is applied and scaled in further experiments.

3.2. Acceleration and optimization of CLP generation

For acceleration and optimization purposes of hydrophobic surface generation, the following investigation is done at a larger beam waist radius w_0 = 40 µm by setting a smaller beam diameter at the scanning aperture. The micro cones grow with increasing number of scans until the roughness and accordingly the height stagnates at S ≈ 25 (Fig. 3a) [25]. Therefore, the effect of varying scanning velocity - accordingly N_{eff} - on the distribution of the cones is examined. The surface roughness parameters and qualitative observation of the textured surfaces indicate an optimal N_{eff} ≈ 900 (F_0 = 4.5 J/cm²). At this parameter setting (encircled in Fig. 3b) Spk and Sz are comparatively high and Smr,1 is about 15 %. For scanning speeds below 1.0 m/s melt bridges occur. Therefore, this morphology would interrupt the air interlayer and should not be suitable to achieve maximum contact angles respectively minimum wettability. Above 2.0 m/s cones are only generated locally. The maximum applied v_S = 8.0 m/s results in nearly homogeneous ripple formation respectively low surface roughness as well as high Smr,1.

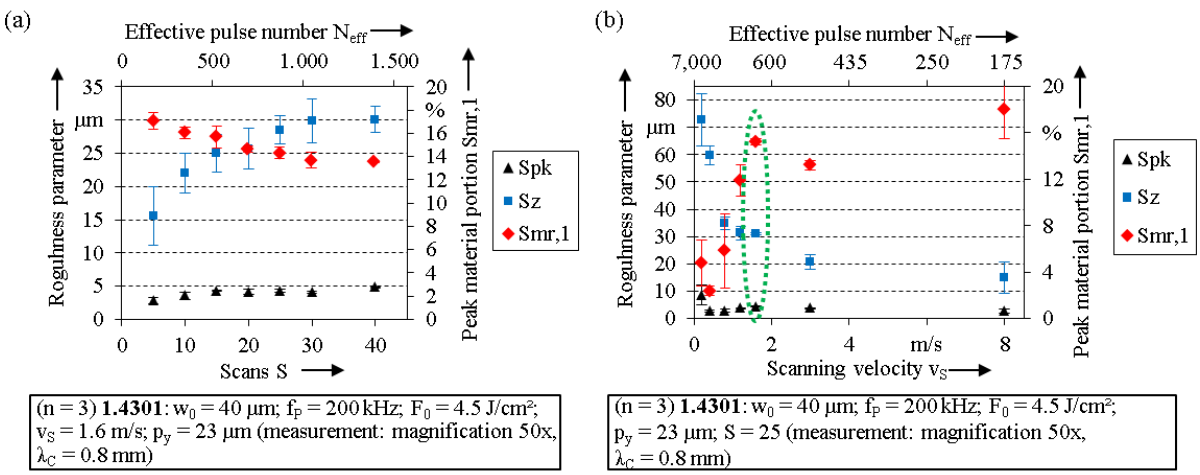

Fig. 3. Roughness parameters of textured surfaces depending on (a) the number of scans S and (b) the scanning velocity v_S

After this parameter study, the general correlation between the formation of homogeneous distributed micro cones and the effective pulse number per unit area respectively the accumulated fluence can be summed up for picosecond laser texturing. Further experimental results under the variation of the spot diameter show generated morphologies of equal surface roughness. Therefore, almost independent from spot diameter an accumulated fluence F_{acc} between 2,600 J/cm² and 3,500 J/cm² leads to rising micro cones height due to hydrodynamic effects [11]. Depending on pulse frequency and heat accumulation, the peak fluence and the scanning velocity have to be set to reach the temperature threshold of self-organized cone formation. In the case of f_P = 200 kHz the velocity should ensure a pulse overlap of approximately 90 %. However, it has to be chosen to a minimum to allow a maximum number of scans for a constant effective number of pulses, because the increase of scans results in increasing height, width and mean distance of the micro cones.

3.3. Morphology and material-dependent contact angle and surface energy

The influence of the surface morphology resulting from different accumulated fluences on the wettability is assessed by contact angle measurements with distilled water on stainless steel 1.4301. Each laser textured surface with its characteristic surface roughness (Fig. 4a) shows similar temporal behavior of the contact angle. Directly after laser processing the contact angle is lower than the one measured on the untreated surface. With increasing temporal interval between laser processing and the contact angle measurement the contact angle increases until it reaches a stead state after about 16 days (Fig. 4b). This maximum value is above the value of the untreated surface. However, depending on the morphology the three variants of textured surfaces reach different maxima.

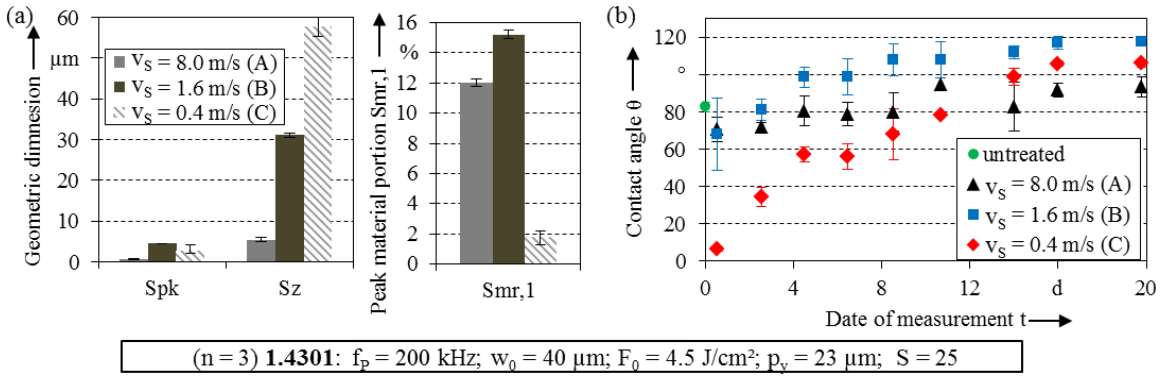

Fig. 4. (a) Roughness parameters of three different morphologies and (b) time depending contact angles on stainless steel 1.4301

The highest contact angle is measured on the surfaces covered with homogeneous micro cones (B) (Fig. 5b). Slightly lower contact angles are found on textured surfaces with broad cones and partially melt bridges (C) (Fig. 5c) which have an higher maximum surface height Sz and significantly lower Smr,1 than the before mentioned surfaces. The third laser-induced morphology (A) (Fig. 5a) with its significantly lower Sz shows the smallest contact angles at the steady state, because this morphology differs drastically from defined cone-like topography according to the *Cassie* model. Thus, the necessity of homogeneous micro cones on surfaces with low wettability can be confirmed.

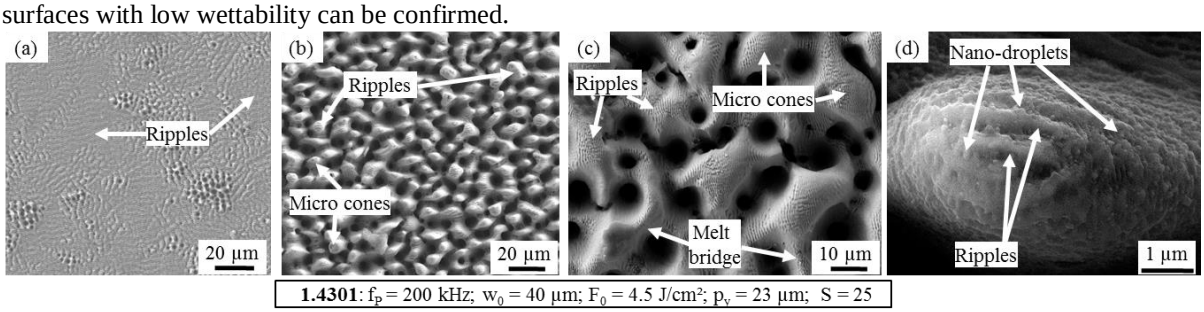

Fig. 5. SEM pictures of the morphology of laser textured surfaces processed with different scanning velocities: (a) v_S = 8.0 m/s, (b) v_S = 1.6 m/s, (c) v_S = 0.4 m/s and (d) view on a single micro cone of surface (B) with nano-droplets and ripples

The detailed observation of the textured morphologies shows that the wettability is realized by a dual-scale structure, which consists of the discussed micro-scaled cones and nano-scaled ripples and droplets on top of the cones (Fig. 5d). These nano-droplets exist on the surfaces with maximum contact angle as well as on the

inhomogeneous ones (C) on 1.4301 (Fig. 5c). At the bottom between the micro cones ripples occur, which are generated by interfering reflected and scattered laser light (Fig. 5b). Ripples with the same periodicity below the wavelength are covering the surface (A) on 1.4301 and prevent complete wetting of the surface (Fig. 5a).

For the evaluation of the influence of the material on the wettability three different steel alloys are investigated, furthermore. The surfaces of the alloys are laser textured in that way, that almost the same roughness parameters are realized as for the morphology variant (B) on 1.4301. For this purpose, the scanning velocity is decreased in texturing of the alloy 1.7229. The set v_S = 1.2 m/s ensures an homogeneous formation of micro cones. This adjustment is necessary because of the significantly higher thermal conductivity of 1.7229 in comparison to 1.4301 (Tab. 1). Due to the faster energy transport into the material this higher heat conductivity leads to a lower temperature at the surface of the material. Thus, the hydrodynamics are changed preventing homogeneous cone formation [23]. The third alloy 1.2379 can be processed with the same parameter setting as 1.4301 as both have nearly the same heat conductivity (Tab. 1). Based on these parameter settings, almost the same morphologies are realized on the surfaces of the three steel alloys (Tab. 2). The measured contact angles show low material-dependency. The contact angles on 1.7229 are slightly smaller than on 1.4301 and 1.2379. The wettability of each steel alloy is characterized by contact angles significantly higher compared to the untreated surface.

Table 2. Roughness parameters, contact angles and surface energies of untreated as well as textured surfaces of three different steel alloys measured directly after laser processing and additional storage in CO_2 atmosphere for 20 days (w_0 = 40 µm; f_P = 200 kHz; p_y = 23 µm; v_S = 1.6 m/s (1.7229: v_S = 1.2 m/s); S = 25; n = 2)

Alloy	Untreated surface		Laser textured surface						
			Directly after laser processing					After storage	
	Contact angle θ	Surface energy γ	Reduced peak height Spk	Max. height of surface Sz	Peak material portion Smr,1	Contact angle θ	Surface energy γ	Contact angle θ	Surface energy γ
1.4301	83 ± 3 °	26.8 J/m²	4.40 ± 0.08 µm	31.08 ± 0.47 µm	15.22 ± 0.29 %	20 ± 4 °	96.0 J/m²	118 ± 3 °	12.6 J/m²
1.2379	90 ± 4 °	25.9 J/m²	3.99 ± 0.17 µm	25.72 ± 0.75 µm	12.62 ± 0.90 %	23 ± 7 °	180.2 J/m²	119 ± 4 °	15.3 J/m²
1.7229	80 ± 5 °	28.0 J/m²	5.27 ± 0.16 µm	28.94 ± 1.28 µm	12.65 ± 0.24 %	11 ± 1 °	79.7 J/m²	114 ± 2 °	8.8 J/m²

All three steel alloys have in common, that in comparison with the initial surface the surface energy is drastically reduced due to laser texturing and storing in CO_2 atmosphere. Directly after the laser treatment the textured surfaces show higher surface energy than the untreated surfaces. As the morphology is nearly the same, the chemical composition is investigated in the following. The analysis of the chemical composition confirms former investigations from *Kietzig et al.* [11]. On each textured surface and steel alloy the carbon concentration decreases and oxygen concentration increases due to laser processing, firstly (Fig. 6a). The increase of the contact angle over storage time can be ascribed to the increase of carbon concentration, which is observable for each steel alloy (Fig. 6b). Depending on the three kinds of laser induced morphologies on 1.4301 the percentage change of carbon and oxygen concentration slightly differs, which can be ascribed to the different N_{eff} and accordingly the accumulated fluences (Fig. 6a). An increase of the accumulated fluence by decreasing the scanning velocity results in more oxidic and less carbonaceous surfaces due to temperature sensitive oxidation of metals [26]. The lower oxygen deficiency leads to higher surface energy and lower contact angles directly after laser texturing (Fig. 4b). Contact angle steady state on the surfaces (C) on 1.4301 is achieved after longer storage time compared to the surfaces (A) and (B) due to the initial higher oxygen and/or lower carbon concentration (Fig. 6a). Depending on the material the percentage change of carbon and oxygen concentration is almost the same (Fig. 6b).

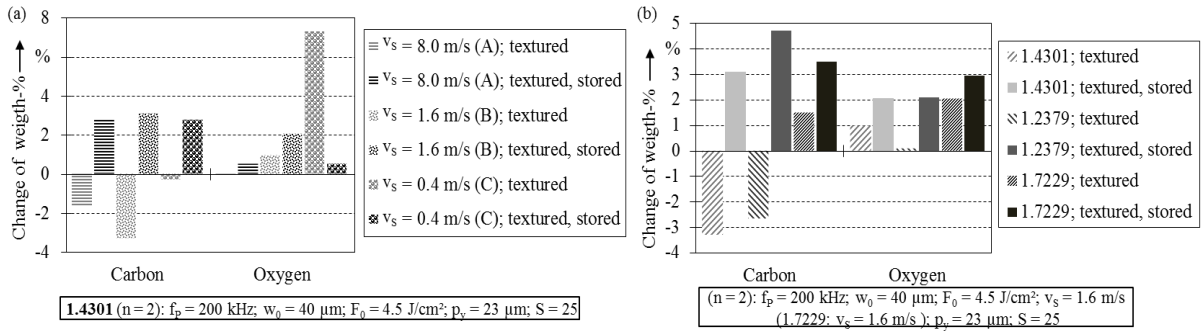

Fig. 6. Change of the chemical composition in comparison to the initial untreated surface regarding carbon and oxygen depending on (a) the surface morphology on 1.4301 and (b) the steel alloy

In combination the morphology and the carbonaceous composition of the laser textured surfaces of different steel alloys induce hydrophobicity and allow a decrease of the surface energy. The slight variation of both properties causes the observed material- and processing parameter-dependent differences of the wetting behavior. The chemical composition of the textured surfaces represents the main parameter to induce hydropohobicity due to reduction of the surface energy. The generated morphology affects the level of hydrophobicity respectively the contact angle value. Due to the application of picosecond laser pulses and the spot diameter d_0 = 80 µm the processing speed is increased compared to the femtosecond-based generation of hydrophobic surfaces consisting of self-organized microstructures.

4. Conclusion and outlook

Picosecond laser texturing is a suitable process to decrease surface energy of steel alloys. Due to the generation of cone-like protrusions with height $H \approx 30$ µm the Wenzel state is achieved during wetting of the textured surfaces. First of all, the necessary low surface energy is induced by the approved accretion of carbon at the textured surfaces. The time-dependency of this accretion causes a delayed hydrophobic steady state of about 16 days. It is found out, that the roughness parameters Spk and Smr,1 are suited to describe the surface topography regarding the height and the distribution of micro cones, which affect the achievable static contact angle. Surfaces of low wettability are characterized by high peak material portion $Smr,1 \geq 15$ %. Further, the contact angle on these surfaces increases by increasing reduced peak height. Regarding CLP formation, a peak fluence of about $F_0 = 4.5$ J/cm² and an effective pulse number $N_{eff} \approx 900$ are necessary to generate surfaces with these roughness values with laser pulses of $\tau = 10$ ps. This parameter combination mainly depends on the heat accumulation so that the scanning velocity is limited to a spot-dependent maximum speed where CLP start to arise. This scanning velocity should enable an overlap of successive laser pulses of approximately 90 %. The application of picosecond laser pulses and the beam waist radius $w_0 = 40$ µm enables the accelerated processing of hydrophobic surfaces compared to femtosecond laser based generation of CLP.

As the chemical properties of the textured surfaces are most important for surface wettability the elemental increase of oxygen and decrease of carbon during the laser ablation process depending on the atmosphere should be a subject of further investigations. Regarding tribological applications, the mechanical properties and tribological behavior of the textured surfaces have to be investigated to determine the applicability of the generated morphologies on surfaces of friction partners.

Acknowledgements

The authors gratefully acknowledge funding of the project “Lubrication free forming with tailored tribological conditions” within the DFG priority programme 1676 “Dry metal forming - sustainable production through dry processing in metal forming” and the funding of the Erlangen Graduate School in Advanced Optical Technologies (SAOT) by the German National Science Foundation (DFG) in the framework of the excellence initiative.

References

[1] Czichos, H; Habig, K.H., 2010: Tribologie-Handbuch: Tribometrie, Tribomaterialien, Tribotechnik. 3., überarb. u. erw. Aufl.
[2] Zhang, Yong-Lai; Xia, Hong; Kim, Eunkyoung; Sun, Hong-Bo, 2012: Recent developments in superhydrophobic surfaces with unique structural and functional properties, Soft Matter 8 (44), p. 11217-11231.
[3] F. Zhang, L. Zhao, H. Chen, S. Xu, D. G. Evans, and X. Duan, Angew, 2008. Corrosion resistance of superhydrophobic layered double hydroxide films on aluminum, Chem. Int. Ed. 47, p. 2466.
[4] Frank, M.A.; Boccaccini, A.R.; Virtanen, S., 2014: A facile and scalable method to produce superhydrophic stainless steel surface, Appl. Surf. Sc. 311, p. 753–757.
[5] Wenzel, R. N., 1936: Resistance of solid surfaces to wetting by water, Industrial and Engineering Chemistry 28 (8), p. 988–994.
[6] Quéré, D., 2008: Wetting and roughness, Annu. Rev. Mater. Res.38, p. 71-99.
[7] Cassie, A.B.D.; Baxter, S., 1944: Wettability of porous surfaces, Transactions of the Faraday Society, p. 1–6.
[8] Bhushan, B., Jung, Y.C., Koch, K., 2009: Micro-, nano- and hierarchical structures for superhydrophobicity, self-cleaning and low adhesion, Philosophical transactions. Series A, Mathematical, physical, and engineering sciences 367, p. 1631–1672.
[9] Li, J.C., Mia, C., Hui, D.Z., Jian, M.C., 2008: Preparation of super-hydrophobic surface on stainless steel, Appl. Surf. Sc. 255, p. 3459-3462.
[10] Pozzato, A., et al., 2006: Superhydrophobic surefaces fabricated by nanoimprint lithography. Microelectr. Eng. 83, p. 884-888.
[11] Tanvir Ahmmed, K.M.; Grambow, C., Kietzig, A.-M., 2014: Fabrication of Micro/Nano Structures on Metals by Femtosecond Laser Micromachining. Micromachines 5, p. 1219-1253.
[12] Cerro, Daniel Arnaldo del, 2014: Picosecond pulsed laser microstructuring of metals for microfluidics. Dissertation. University of Twente, Enschede. Faculty of Engineering Technology.
[13] Tang, Min, 2012: Design and Fabrication of super-hydrophobic surfaces by laser micro-nano-processing. Dissertation. National University of Singapore, Singapore.
[14] Kietzig, Anne-Marie, Hatzikiriakos, Savvas G., Englezos, Peter, 2009: Patterned superhydrophobic metallic surfaces. In: Langmuir: the ACS journal of surfaces and colloids 25 (8), p. 4821–4827
[15] Cunha, A., et al., 2013: Wetting behaviour of femtosecond laser textured Ti–6Al–4V surfaces, Appl. Surf. Sc. 265, p. 688-696.
[16] Deutsche Edelstahlwerke GmbH, 2008, Nichtrostender austenitischer Stahl 1.4301, http://www.dew-stahl.com/fileadmin/files/dew-stahl.com/documents/Publikationen/Werkstoffdatenblaetter/RSH/1.4301_de.pdfhttp://www.thyssenkrupp.at/files/rohre/Werkstoffdatenblaetter/1.4301.pdf, (29.04.2015).
[17] Esterer Gießerei, 2011: Werkstoffübersicht. unter Mitarbeit von H. Oswald. http://www.esterer-giesserei.de/fileadmin/user_files/pdf/Verguetungsstahlguss__GS_.pdf (29.04.2015).
[18] Dörrenberg Edelstahl GmbH, 2008, 1.2379 X153CrMoV12, 1.4301http://www.doerrenberg.de/uploads/tx_c1x1downloads/1.2379_de.pdf (29.04.2015).
[19] König, J., S. Nolte, and A. Tünnermann, 2005: Plasma evolution during metal ablation with ultrashort laser pulses, Opt. Express 13(26), p. 10597-10607.
[20] DIN EN ISO 25178, 2011: Geometrische Produktspezifikation (GPS) - Oberflächenbeschaffenheit Flächenhaft. Berlin, Beuth
[21] DIN 55660-2, 2011: Bestimmung der freien Oberflächenenergie fester Oberflächen durch Messung des Kontaktwinkels. Berlin, Beuth
[22] Liu, B., et al., 2013: Formation of Porous Structure with Subspot Size under the Irradiation of Picosecond Laser Pulses. J. of Nanomat. 2, p. 1-9.
[23] Tanvir Ahmmed, K.M., et al., 2015: Introducing a new optimization tool for femtosecond laser-induced surface texturing on titanium, stainless steel, aluminum and copper, Opt. and Lasers in Eng. 66, p. 258-268
[24] Bauer, F.; Michalowski, A.; Kiedrowski, T.; Nolte, S., 2015: Heat accumulation in ultra-short pulsed scanning laser ablation of metals, Opt. Express 23 (2), p. 1035–1043.
[25] Kam, B.H., Bhattacharya, S., Mazumder, J., 2012: Control of the wetting properties of an AISI 316L stainless steel surface by femtosecond laser-induced surface modification, J. Micromech. Microeng. 22, p. 105019 (6pp).
[26] Young, D.J., 2008: High Temperature Oxidation and Corrosion of Metals, Elsevier (1), p. 1-574.